Journal of Thermal Analysis and Calorimetry, Vol. 70 (2002) 755–795

THERMAL ANALYSIS OF ENVIRONMENTALLY COMPATIBLE POLYMERS CONTAINING PLANT COMPONENTS IN THE MAIN CHAIN

H. Hatakeyama[*]

Fukui University of Technology, Department of Applied Physics and Chemistry, Graduate School of Engineering, 3-6-1, Gakuen, Fukui 910-8505, Japan

Abstract

Environmentally compatible polymers such as poly(ε–caprolactone) (PCL) and polyurethane (PU) derivatives from PCL's were synthesized from saccharides, polysaccharides and lignins such as glucose, fructose, sucrose, cellulose, cellulose acetate, alcoholysis lignin, kraft lignin and sodium lignosulfonate. Flexible and rigid PU sheets and foams were also prepared by the reaction of OH groups of saccharides and lignins with isocyanates such as toluene diisocyanate (TDI) and diphenylmethane diisocyanate (MDI). Glass transition temperatures (T_g's), cold-crystallization temperatures (T_{cc}'s) and melting temperatures (T_m's) of saccharide- and lignin-based PCL's and PU's were determined by differential scanning calorimetry (DSC), and phase diagrams were obtained. Methods of controlling mechanical properties such as stress and elasticity of PU's through changing thermal properties such as glass transition temperature were established. Thermogravimetry (TG) and TG-Fourier transform infrared spectrometry (FTIR) were also carried out in order to analyze the degradation temperature and evolved gases from the above obtained polymers.

Keywords: lignin, poly(ε-caprolactone), polyurethane, saccharide, thermal analysis

Introduction

Natural and synthetic polymers are indispensable in the modern human life. Recently, however, it has been found that most synthetic polymers that have been developed by using petroleum and coal as raw materials are not compatible with the environment, since they cannot be included in the natural recycling system.

Modern societies have serious problems of contradictions between the convenience of human life and compatibility to natural circumstances. It is easy to say that we have to return to nature in order to solve the problems coming from man-made materials. However, this means that we lose all the convenient features and materials which science has developed through human history.

Accordingly, in the present polymer industry, polymers that are compatible to natural circumstance are the key to sustainable developments that can keep the rich and con-

* Author for correspondence: h-hatake@ccmails.fukui-ut.ac.jp

1418–2874/2002/ $ 5.00

Akadémiai Kiadó, Budapest
Kluwer Academic Publishers, Dordrecht

venient life developed by science. One possible way of the development of environmentally compatible polymers is the preparation of biodegradable polymers. Table 1 offers an overview of biodegradable polymers that have recently been developed.

Table 1 Overview of biodegradable polymers

Type of polymers	Example of polymers
Poly(α-ester)s	poly(glycolic acid) (PGA) derivatives poly(lactic acid) (PLA) derivatives copolymers of PGA and PLA
Poly(hydroxyalkanoate)s	poly(3-hydroxybutyrate) (P3HB) poly(4-hydroxybutyrate) (P4HB) poly(3-hydroxyvalerate) (P3HV)
Polylactones	poly(ε-caprolactone) poly(valerolactone)
Saccharide-based polymers	saccharide-based-poly(ε-caprolactone) derivatives saccharide-based polyurethanes
Cellulose-based polymers	cellulose-acetates cellulose-based poly(ε-caprolactone) derivatives
Lignin-based polymers	lignin-based poly(ε-caprolactone) derivatives lignin-based polyurethanes
Starch-based polymers	blends
Chitin- and chitosan-based polymers	polymeric derivatives and composites
Other synthetic polymers	polyvinyl(alcohol and acetates)

For the development of environmentally compatible polymers, it is essential to understand that nature constructs a variety of materials which can be used in human life. Saccharides have already been used extensively in the food, medical and cosmetic industries. Plant materials such as cellulose, hemicellulose and lignin are the largest organic resources. However, they are not very well used except for cellulose. Hemicellulose has not yet been utilized. Lignin, which is obtained as the by-product of pulping industry, probably over twenty million tons per year in the world, is mostly burnt as fuel and only increases the amount of carbon dioxide in the environment, although lignin is one of the most useful natural resources.

Biomaterials span the range from elastic solids to viscous liquids. The complexity indigeneous to biomaterials is based on the intricacies of their molecular architecture. However, scientific advances enable us to understand molecular features of biomaterials through modern analytical methods such as infrared spectroscopy, nuclear magnetic resonance spectroscopy, thermal and mechanical analysis, and electron microscopy. Now it is the time to consider that the compounds produced through biosynthesis can be used as half-made up raw materials for the synthesis of useful plastics and materials in human life. Major plant components, such as saccharides and lignin, contain highly reactive hydroxyl groups which can be used as reactive chemical reaction sites. As shown in Fig. 1, using the reaction sites, it is possible to convert saccharides and lignin, for exam-

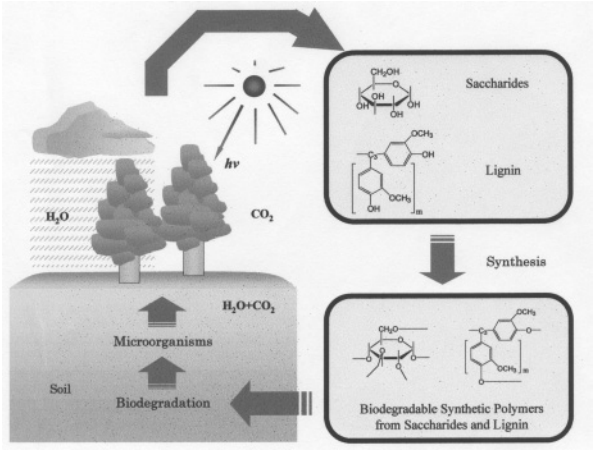

Fig. 1 Recycling of environmentally compatible polymers containing plant components

ple, to gels, membranes, functional polymers, engineering plastics and biodegradable polymers that are environmentally compatible [1–30].

This paper is concerned with thermal properties of environmentally compatible polymers derived from saccharides and lignins. The above research results have been obtained over the last several years by our coworkers working at different institutions. The above environmentally compatible polymers include polymers such as poly(ε-caprolactone) (PCL) and polyurethane (PU) derivatives. PCL derivatives were synthesized from lignin, saccharides, cellulose and cellulose acetate. PU derivatives were prepared from saccharides and lignins. Thermal properties of the above polymers were studied by differential scanning calorimetry (DSC), thermogravimetry (TG) and TG-Fourier transform-infrared spectrometry (FTIR).

Methods of characterization

Differential scanning calorimetry (DSC)

DSC is a useful technique for studying thermal behaviour of newly synthesized polymers containing plant components in the molecular chain. For example, PU's are usually cross-linked and amorphous polymers except PU's with highly crystalline molecular chains such as PCL. DSC can be used to identify phase transitions such as glass transition, cold crystallization and melting temperatures (T_g, T_{cc} and T_m) during heating process. Observed exo- and endotherms can be used to calculate enthalpy changes occurring with phase transitions. The following process is an example of DSC measurements performed at our laboratory.

DSC was carried out on all prepared samples using a Seiko DSC 220C in N_2 atmosphere. The scanning rate was usually 10°C min^{-1}. Before carrying out the measurements, the samples were dried in an air-oven at 120°C for 2 h. T_g was defined as the temperature at the point of intersection between the tangents drawn at the point of inflection of the transition and at the flat part of the curve before the transition [31]. Heat capacity differ-

ence at T_g was measured. Phase transition temperatures such as T_{cc} and T_m were also defined [31]. Enthalpy of the first order phase transitions was estimated.

Thermogravimetry (TG)

TG is a useful technique for studying thermal degradation of environmentally compatible polymers, since thermal stability from the view point of practical applicability in various fields can be evaluated by this method. The following process is an example of TG measurements performed at our laboratory.

TG-curves of all the samples were recorded using a Seiko TG/DTA (differential thermal analysis) 220. The curves were obtained at a heating rate of 10°C min^{-1} in a nitrogen atmosphere (30 mL min^{-1}). In order to examine the effect of atmosphere on decomposition behaviour, the TG curves were also obtained in air. The thermal degradation temperature (T_d) of these materials is defined as the temperature at the point of intersection of the tangents drawn from a point before the main decomposition step (i.e. where the curve is horizontal) and from the point of inflection of the main step [31].

TG-Fourier transform infrared spectrometry (TG-FTIR)

TG-FTIR is a method to characterize compounds contained in evolved gases from thermally degraded samples. The following process is an example of TG-FTIR measurements performed at our laboratory.

TG-FTIR was performed using a Seiko TG 220 thermogravimeter equipped with a JASCO FTIR 7000 spectrometer. TG measurements were carried out at a heating rate of 20°C min^{-1}. Nitrogen and air flow rates were controlled at 100 mL min^{-1}. The evolved gases during thermal degradation were simultaneously analyzed by FTIR. In order to obtain one spectrum, data of ten scans with a scan interval of 1 s were accumulated. Each spectrum was recorded every 30 s. The resolution of spectra was 1 cm^{-1}.

Dynamic mechanical analysis (DMA)

The relaxation behaviour of polymers was studied as functions of temperature and frequency. Changes in the dynamic storage modulus, E' and the dynamic loss modulus, E'' were obtained. For viscoelastic polymers such as saccharide- and lignin-based PCL and PU derivatives, E' characterizes the ability of the polymer to store energy (elastic behaviour), while E'' reveals the tendency of the material to dissipate energy (viscous behaviour). The phase angle is calculated from $\tan\delta = E''/E'$. The following process is an example of DMA measurements performed at our laboratory.

Dynamic mechanical analysis was carried out using a Seiko DMS 200. The samples were 20 mm long and had a cross sectional area of approximately 3.5 mm^2. In order to eliminate a trace amount of water in the sample which sorbed during sample handling, the sample clamped between two holders was heated to 150°C, maintained for 5 min and then quenched to –150°C. DMA measurements were carried out in the bending mode in a temperature ranging from –150°C to 200°C at different frequencies. The scanning rate was 1°C min^{-1}.

Preparation of materials

Polycaprolactone derivatives

Polycaprolactone derivatives from saccharides

Saccharide-based PCL's were synthesized by the polymerization of ε-caprolactone (CL) which was initiated by each OH group of glucose, fructose and sucrose. The amount of CL was varied from 1 to 5 moles per OH group of each saccharide. The polymerization was carried out for 12 h at 150°C with the presence of a small amount of dibutyltin dilaurate (DBTDL).

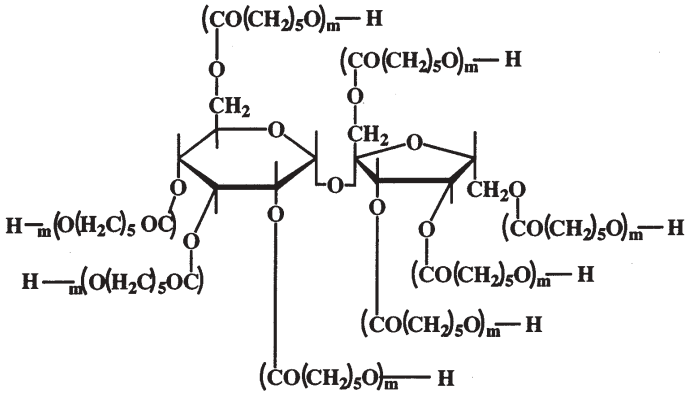

Fig. 2 Schematic chemical structure of sucrose-based PCL's

Figure 2 shows the schematic chemical structure of sucrose-based PCL's. The results of the characterization of glucose- (Glu-), fructose- (Fru-) and sucrose-(Suc-)based PCL's have been reported elsewhere [27].

Polycaprolactone derivatives from cellulose acetate (CA)

CAPCL's were synthesized from cellulose acetate (Kodak Co. Ltd, CA; acetyl content, 39.87%; M_w=6.32·10^4; M_w/M_n=2.27). Distilled CL, which was dehydrated in benzene by reflux method, was added to dried CA and polymerization was carried out for 22 h at 150°C with the presence of a small amount of dibutyltin dilaurate (DBTDL) as a catalyst. CL/OH (mol mol^{-1}) ratios were varied from 2 to 20 (mol mol^{-1}) (CL/OH ratio=2, 5, 8, 10, 15, 20). When the polymerization of the samples with CL/OH ratio was 2 and 5, N-methylpyrrolidone was used as a solvent in order to have a viscous media. The above CA-PCL's were dissolved in hot acetone and then put in methanol dropwise. Precipitates in flake shape were obtained. Samples were dried in an oven in vacuum at 105°C for 12 h. Flake-shaped samples were pressed at 100 kg cm^{-2} at 180°C for 10 min. Figure 3 shows a schematic chemical reaction for the synthesis of CAPCL.

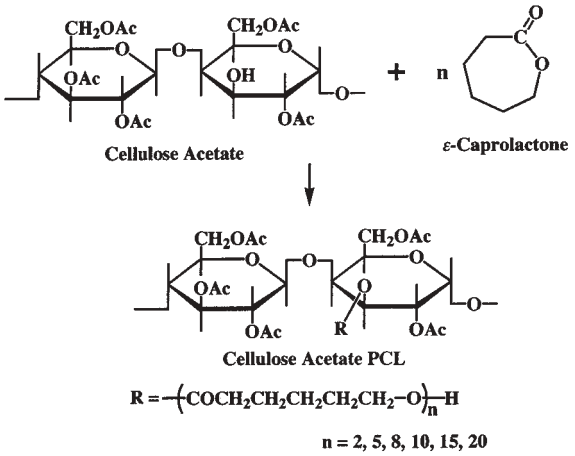

Fig. 3 Schematic chemical reaction for the synthesis of CAPCL

Polycaprolactone derivatives from cellulose

Cellulose-based polycaprolactone derivatives (CellPCL's) were synthesized by 2-step reactions. In the first step, cellulose powder was suspended in N,N-dimethylacetoamide (DMAc) and cellulose soaked with DMAc was obtained by filtration. The above cellulose soaked with DMAc was dissolved in DMAc solution of lithium chloride (LiCl), dehydrated by refluxing with benzene and then was reacted with CL with the presence of a small amount of triethylamine as a catalyst. CL/OH (mol mol^{-1}) ratio was 0.33 at this stage. The above obtained cellulose-CL derivative was dissolved in N-methylpyrrolidone. Distilled CL was added to the above solution and the polymerization was carried out for 22 h with the presence of a small amount of DBTDL as a catalyst. CL/OH ratios were varied from 0.66 to 5 mol mol^{-1}. Precipitates in flake shape were obtained by putting the DMAc solution of CellPCL's obtained above into methanol. Figure 4 shows a schematic chemical structure of cellulose-based PCL.

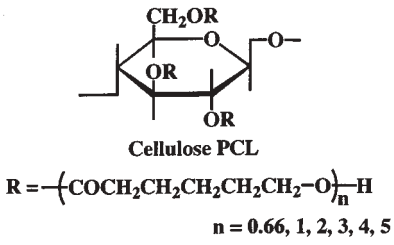

Fig. 4 Schematic chemical structure of cellulose-based PCL

Polycaprolactone derivatives from lignins

Alcoholysis lignin (AL) (Alcel lignin®) was provided by Repup Technologies Inc., and kraft lignin (KL) was commercially obtained from Westvaco Co. Ltd. PCL with molecular mass $1.0 \cdot 10^4$ was purchased from Wako Pure Chemical Co. Ltd., Japan as

a reference material. PCL in pellet form was pressed at 120°C under the pressure of 10 MPa using a Tester Industry Hot Presser SA-302.

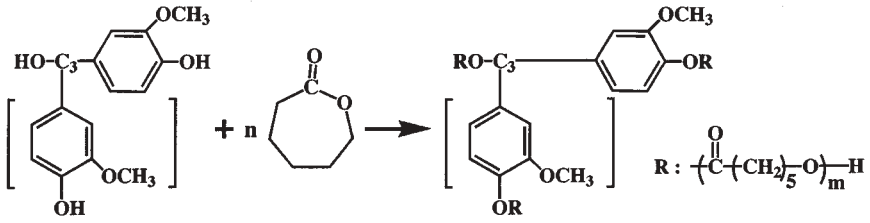

Fig. 5 Schematic chemical structure of lignin-based PCL

Alcoholysis lignin-based PCL (ALPCL) and kraft lignin-based PCL (KLPCL) were synthesized by polymerization of CL which was initiated by the hydroxyl (OH) group of the lignins. The amount of CL was varied from 1 to 25 moles per OH group of each lignin (CL/OH ratio=1, 2, 3, 4, 5, 10, 15, 20 and 25 mol mol^{-1}). The polymerization was carried out for 12 h at 150°C with the presence of a small amount of DBTDL. ALPCL and KLPCL sheets were prepared by heat-pressing the synthesized polymers at 160–180°C at ca 10 MPa. A schematic chemical reaction for the synthesis of LigPCL is shown in Fig. 5.

Polyurethane (PU) derivatives

PU derivatives from saccharides

Saccharide-based PU sheets

Due to the limited solubility of saccharides such as glucose, fructose and sucrose in polyethylene glycol (PEG), the saccharides were first dissolved in PEG 200 (molecular mass 200) or PEG 400 (molecular mass 400) at 50 or 60°C.

Prior to reaction with diphenylmethane diisocyanate (MDI, the isocyanate content of the pure MDI was 6.75 mmol g^{-1}, provided by Mitsui Toatsu, Chem. Industry), the polyol solutions of saccharides were dried under vacuum with vigorous stirring at 75°C for 1 h. Depending on the saccharide content, 0.20–0.50% of total mass of a 1% solution of DABCO in diethylene glycol (DEG) was added to the polyol solution as a catalyst. The amount of catalyst was adjusted so as to achieve a required prepolymerization time of approximately 10 min before the viscosity increased to a desirable level. MDI was added and the reaction was allowed to proceed at room temperature with moderate stirring. The NCO/OH (moles of isocyanate group/moles of OH groups) ratio was changed from 1.0 to 1.2, depending on the required physical properties of prepared PU sheets. During the second half of the pre-polymerization, the system was evacuated using a vacuum pump.

The pre-polymerized mixture was poured into a teflon coated mold and placed in a hot press at 120°C at a pressure of 10 MPa and subsequently in an air-oven between two glass plates (to avoid bending) at 120°C. The total curing time was 25 h. The hot press

used, was purchased from Tester Sangyo Co., Ltd., Japan. Approximately 40 g of material was needed to prepare one sheet of dimensions of 1×140×140 mm.

Molasses-based PU foams

Flexible PU foams were prepared from molasses-polyol, which was a solution of molasses in PEG 200, by polymerization with polypropylene glycol (PPG 3000, molecular mass 3000), toluene diisocyanate (TDI, provided by Mitsui Toatsu Chemical Co. Ltd) and MDI. Molasses was obtained from Syonan Sugar Manufacture Co. Ltd. PEG and PPG were obtained from Daiichi Chemical Industry Co. Ltd. Silicon type surfactant was obtained from Nippon Unicar Co. Ltd. Sn type catalyst (tin octanoate) was supplied by Jyohoku Chemical Industry Co. Ltd, and amine catalyst (pentamethyl-diethylenetriamine) was obtained from Wako Pure Chemical Industry Co. Ltd.

Polyol solutions of molasses were prepared by mixing molasses and PEG 200 at various mixing ratios. The hydroxyl group content of molasses polyol (MP) was determined according to JIS K 1557. In order to prepare PU foams, predetermined amount of PPG 3000 was added to MP. Then calculated amounts of TDI or MDI, surfactant, catalysts and a trace amount of water as a foaming agent were added to MP and PPG mixture under vigorous stirring. Foaming was carried out immediately after removing the stirrer. The obtained foam was cured overnight at room temperature.

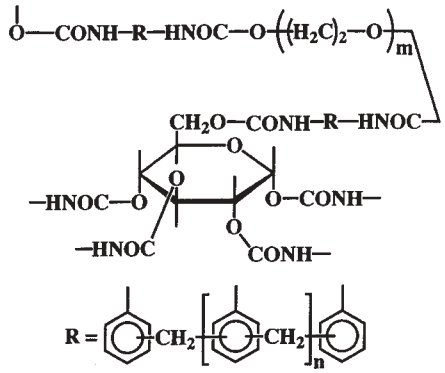

Fig. 6 Schematic chemical structure of saccharide-based PU

Three kinds of model polymers having unit structures composed of the above samples were also prepared as reference materials i.e., PU foams from PEG 200, PPG 3000 and molasses polyol (33% molasses in PEG 200) with PPG 3000 were prepared using the same procedure as mentioned above. They are abbreviated as PEG-PU, PPG-PU and Molasses-PU, respectively. A schematic chemical structure of the PU sample with saccharide structure is shown in Fig. 6.

PU derivatives from lignins

Various kinds of industrial lignins were used as raw materials for the preparation of lignin-based PU's at our laboratory. Hardwood solvolysis lignin (SL) was obtained as

a by-product in organosolve pulping of Japanese beech (*Fagus crenata*) with aqueous cresol at 185°C without an acid catalyst. The SL was provided by the Japan Pulp and Paper Research Institute Co. Ltd. Sodium lignosulfonate (LS) was provided by Nippon Paper Industries Co., Ltd. Poly(ethylene glycol) (PEG), poly(propylene glycol) (PPG) and diphenylmethane diisocyanate (MDI) were obtained as previously stated.

The following methods are examples of preparation of lignin-based PU's. Prior to obtaining PU's, KL, AL, SL and LS were dissolved in polyols such as PEG and PPG in order to prepare polyol solutions containing lignin. The obtained polyol solutions were mixed with MDI and plasticizer (PEG or PPG) at room temperature, and precured polyurethanes were prepared. Each of the precured polyurethanes was heat-pressed and a PU sheet was prepared. In order to prepare PU foams, first the above polyol solution was mixed with plasticizer, surfactant (silicone oil), and a catalyst (DBTDL), and then MDI was added. This mixture was vigorously stirred with a trace amount of water which was added as a foaming agent. In the above processes, the NCO/OH ratio, the mass of starting materials and the contents of lignin (shown as Lig in the following equations), the amount of polyols such as PEG and PPG (shown as PEG in the following equations), and MDI were calculated according to the following equations:

$$\text{NCO/OH}=M_{\text{MDI}}W_{\text{MDI}}/(M_{\text{Lig}}W_{\text{Lig}}+M_{\text{PEG}}W_{\text{PEG}})$$

$$W_{\text{t}}(g)=W_{\text{Lig}}+W_{\text{PEG}}$$

$$\text{Lignin content/\%}=(W_{\text{Lig}}/W_{\text{t}})100$$

$$\text{PEG content/\%}=(W_{\text{PEG}}/W_{\text{t}})100$$

where M_{MDI} is the number of moles of isocyanate groups per gram of MDI, W_{MDI} the mass of MDI, M_{Lig} the number of moles of hydroxyl groups per gram of lignin, W_{Lig} the mass of lignin, M_{PEG} the number of moles of hydroxyl groups per gram of PEG, W_{PEG} the mass of PEG, and where W_{t} is the total mass of lignin and PEG in the PU system. In some cases, DEG was used instead of PEG.

A schematic chemical structure of the PU sample containing lignin structure is shown in Fig. 7.

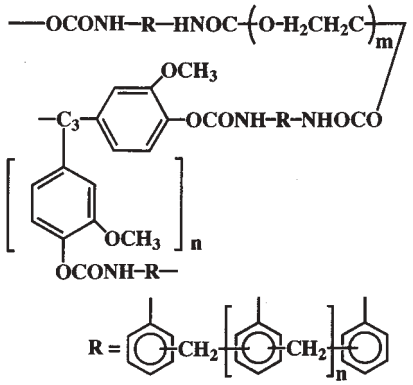

Fig. 7 Schematic chemical structure of lignin-based PU

PU's derived from saccharide- and lignin-based PCL's

PU's derived from saccharide-based PCL's

Polyurethane sheets were obtained from saccharide-based PCL's by the following procedure. Saccharide-based PCL's were dissolved in tetrahydrofuran (THF). MDI was reacted with the above solution for 30 min at room temperature with stirring. The obtained prepolymer was cast on a glass plate and the solvent was evacuated in a desiccator under dry conditions. The obtained polyurethane sheet was cured at 120°C for 2 h.

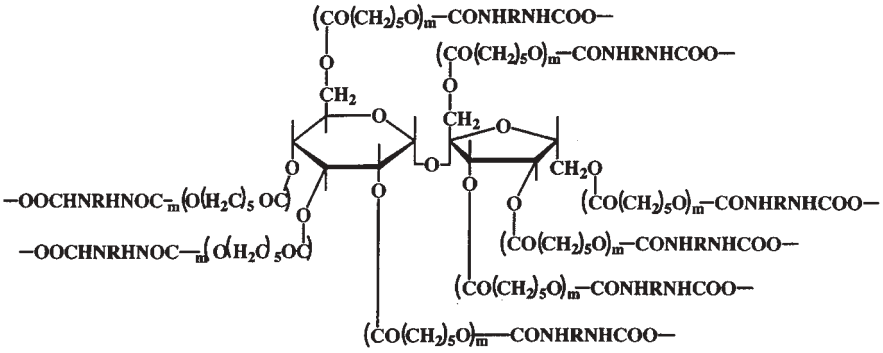

Fig. 8 Schematic chemical structure of PU derived from sucrose-based PCL's

The core structure of prepared PU's consists of saccharide-based PCL's linked by urethane bonding. Accordingly, it can be assumed that the obtained PU's are essentially copolymers having three-dimensional networks of urethane bonding which have saccharide-based PCL components. A schematic chemical structure of PU's derived from SucPCL is shown in Fig. 8, as an example of prepared PU's.

PU's derived from lignin-based PCL's

PU samples of ALPCL and KLPCL were obtained by the following procedure. Lignin-based PCL's were dissolved in tetrahydrofuran (THF). Diphenylmethane

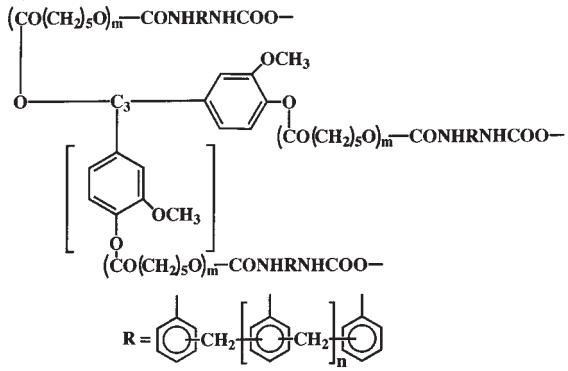

Fig. 9 Schematic chemical structure of PU derived from lignin-based PCL's

diisocyanate (MDI) was reacted with the above solution for 30 min at room temperature with stirring. The obtained prepolymer was cast on a glass plate and the solvent was evacuated in a desiccator under dry conditions. The obtained ALPCL-based PU and KLPCL-based PU sheets were cured at 120°C for 2 h. The schematic chemical structures of the sample (Lig PCLPU) are shown in Fig. 9.

Thermal properties

Cellulose acetate-based PCL derivatives

Figure 10 shows stacked DSC heating curves of CA and CAPCL's measured at 10°C min^{-1}. As shown in Fig. 10, a baseline deviation showing glass transition is clearly observed for the CA sample (shown as CL/OH ratio=0) and CAPCL samples. DSC curves were also measured at various heating rates from 2 to 40°C min^{-1} and the heating rate dependency of T_g was clearly observed. It is known that T_g of CA depends mainly on acetyl contents not on molecular mass or molecular mass distribution [32]. T_g of CA observed in this study was 147°C and this value accords well with reported values [16]. Both glass transition and melting can be observed in the DSC curve of PCL. A melting peak of CAPCL was observed at around 50°C. A melting peak of PCL was observed at 67°C. This value accords well with reported values [33]. Accordingly it may be reasonable to consider that the melting peaks observed in Fig. 10 correspond to the melting of the PCL side chain grafted to the OH group of CA.

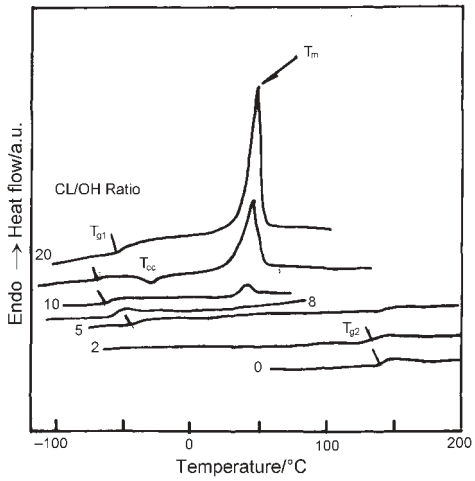

Fig. 10 Stacked DSC heating curves of CA and CAPCL's; T_g: glass transition temperature, T_{cc}: cold crystallization temperature, T_m: melting temperature; Numerals shown in the figure indicate CL/OH ratios; Heating rate: 10°C min^{-1}

Figure 11 shows relationships between T_g's and CL/OH ratio. It is known that dry cellulose shows no glass transition in a temperature from 20°C to thermal decomposition temperature [34]. Previous studies on heat capacity (C_p) measurement of dry

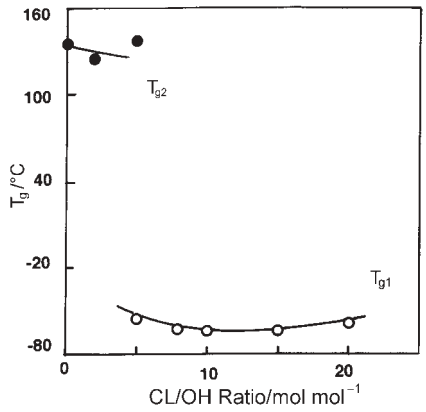

Fig. 11 Relationships between T_g's and CL/OH in CAPCL; o – T_{g1}, ● – T_{g2}

cellulose show that the gradient of C_p increase depends on the crystallinity of cellulose [34]. When the acetyl group is introduced to the cellulose main chain, T_g can be observed as shown in Fig. 10. The above facts suggest that T_g of glucopyranose rings can be observed by the introduction of large side chain molecules such as PCL. When the DSC curves shown in Fig. 10 were magnified, the two baseline deviations due to glass transition of CA and PCL were clearly observed. T_g of CA (T_{g2}) can be observed in the initial stage and becomes difficult to detect when CL/OH ratio exceeds 15 mol mol^{-1}. It is thought that T_g of CA is observable when intermolecular distance expands by the introduction of large side chain molecules, and the geometrical free space enhances the main chain motion of the main chain. T_g of PCL (T_{g1}) decreases in the initial stage and increases slightly after reaching a minimum point at around CL/OH= 10 mol mol^{-1}. The T_g increase observed in the sample with CL/OH ratio 20 suggests that the molecular motion of PCL random chains is restricted by the presence of crystalline region.

As shown in Fig. 10, the melting peak of PCL chains was observed for the PCL samples with CL/OH ratio 10, 15 and 20 mol mol^{-1}. A broad exothermic peak due to cold crystallization (T_{cc}) at –30°C was also observed for the sample with CL/OH ratio 15 mol mol^{-1}. In order to obtain samples having the same thermal history in both DSC and DMA measurements, the samples were heated to 120°C and cooled to –150°C at cooling rate of 40°C min^{-1}. The heating run was carried out at 2°C min^{-1}. By slow heating, T_m shifted to the high temperature side and ΔH_m (J g^{-1}) increased. T_m of the sample with CL/OH ratio 8 mol mol^{-1} became observable, in contrast, T_{cc} was hardly observed in the samples heated at 2°C min^{-1}.

Figure 12 shows the relationships between T_m, ΔH_m and CL/OH ratio. Temperature of melting (T_m) and enthalpy of melting, ΔH_m increase with increasing CL/OH ratio. Both T_m and ΔH_m of the samples heated at 2°C min^{-1} are higher than those heated at 10°C min^{-1}. The results indicate that the higher order structure formation is strongly affected by thermal history, i.e. the crystallinity of PCL chains increases during heating.

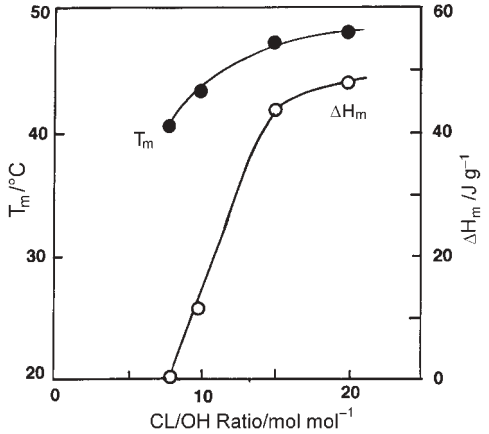

Fig. 12 Relationships between T_m, ΔH_m and CL/OH ratio in CAPCL; ● – T_m, o – ΔH_m

As shown in Fig. 13, the heat capacity difference at T_g (ΔC_p) varies inversely with T_g and the highest value of ΔC_p is observed at around CL/OH ratio 10 mol mol^{-1}. The variation of T_g shown in Fig. 13 suggests that the main chain motion of PCL is enhanced with increasing chain length. At the same time, if PCL long chain molecules form a well arranged crystalline structure, molecular motion of the main chain is restricted.

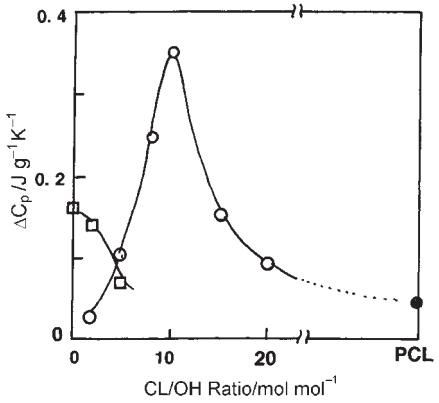

Fig. 13 Relationships between ΔC_p and CL/OH ratio in CAPCL; o – ΔC_p for T_{g1}, □ – ΔC_p for T_{g2}

It is known that a reciprocal relationship is established between T_g and ΔC_p values among a large number of amorphous polymers when the samples are completely random and have no intermolecular bonding [35]. When the relationship between T_g and ΔC_p is discussed for complex polymers, such as CAPCL, it must be taken into consideration that the thermodynamically equilibrium state is not attained in either glassy or rubbery state when ΔC_{ptg} values are measured by dynamic measurement. As shown in Figs 10 and 12, the crystalline region is formed in the samples with high CL/OH ratio. A part of the amorphous region is transformed to the crystalline region

which can be observed as T_{cc}. This means that molecular motion at a temperature higher than T_g of the samples with high CL/OH ratio is restricted and ΔC_p is necessarily small. The fact that ΔC_p values cannot be estimated for the samples heated at 2°C min^{-1} indicates that the number of chain molecules contributing to the enhanced molecular motion is reduced by slow heating. At the same time, a part of the main chain still forms a random structure whose molecular arrangement is similar to that measured at 10°C min^{-1}, since a small baseline inflection can be observed and T_g values show no large difference among the samples having different thermal histories.

Figure 14 shows representative DMA heating curves of CAPCL with CL/OH ratio 5 mol mol^{-1} measured at various frequencies. *E*' (Pa) gradually decreases from –150 to –50°C and a steep decrease is observed at around 100°C. Tanδ shows three peaks as shown in Fig. 14, depending on frequencies. From the high to low temperature side, each tanδ peak was designated as α-dispersion, β-dispersion and γ-dispersion, respectively.

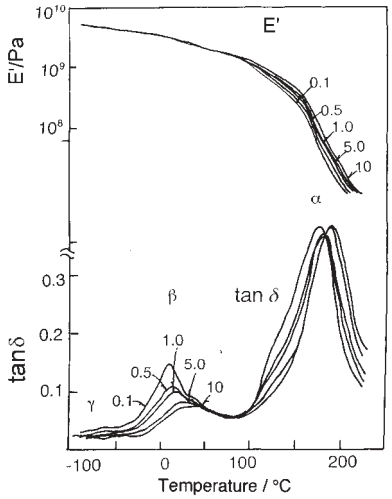

Fig. 14 Representative DMA heating curves of CAPCL with CL/OH ratio 5 mol mol^{-1}; Numerals in the figure indicate frequency (Hz)

When the chain length of PCL increases, β-dispersion becomes marked i.e. intensities of *E*" and tanδ increase and decrease after reaching a maximum. The variation corresponds to the number of amorphous chains concerning β-dispersion. When the crystalline region is formed, the crystallites restrict the incoherent movement of random chains and the number of molecular chains involving enhanced molecular motion decreases. Tanδ values at the peak temperature with CL/OH ratio show a maximum at around CL/OH=8 to 10 mol mol^{-1} [36]. The variation of the intensities of tanδ at the β-dispersion is similar to that of ΔC_p shown in Fig. 13. Both results indicate that the molecular mobility of the main chains is high at around CL/OH ratio 5–10 mol mol^{-1}. When either the side PCL chain length is short or the crystallinity increases, free molecular motion is disturbed.

Activation energy (E_a) of each dispersion was calculated from frequency dependence of maximum temperature of tanδ assuming the applicability of Arrehenius equation. E_a of β-dispersion is shown in Fig. 15. E_a reaches a minimum at around CL/OH ratio=8–10 mol mol^{-1}. As already reported, E_a of the main chain motion ranges from 100 to 250 J mol^{-1} [35]. Accordingly, it is appropriate to consider that β-dispersion is attributed to the main chain motion of the PCL side chain.

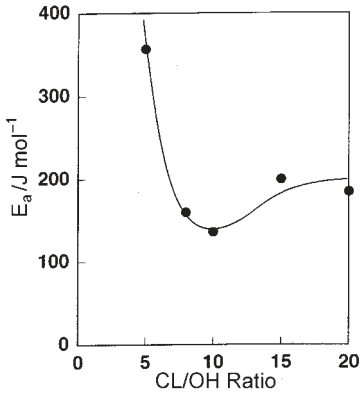

Fig. 15 Relationship between E_a (activation energy of β-dispersion) of CAPCL and CL/OH ratio

From the above results, it can be said that the main chain motion of both CA and PCL chains is observed in a CL/OH ratio 2–10 mol mol^{-1}. PCL chains attached to glucopyranose rings were associated with each other at around CL/OH ratio 8 mol mol^{-1}, and the melting of the crystalline region of PCL chains can be observed at around 50°C. The main chain motion of CA is observable in a low CL/OH ratio, however, it becomes difficult to detect when the crystalline region of PCL is formed. Variation of T_g, temperature of β-dispersion of PCL and ΔC_p indicates that the molecular chains become mobile with increasing CL/OH ratio until CL/OH reaches 10 mol mol^{-1}. After that the main chain motion of PCL is restricted by crystal growth, since sufficiently long chains are assembled to form a crystalline region. The sample with CL/OH ratio 5–10 mol mol^{-1} shows intermediate characteristics, i.e. amorphous structure is formed by cooling from the molten state and cold crystallization is observed during heating. However, when the sample is slowly heated, crystallites were formed. On this account, the difference in T_m's of samples having different heating rates was observed. This suggests that amorphous content and/or crystallinity can be controlled by suitable thermal treatment. This indicates that the degree of freedom of molecular chains decreases with crystal growth. By the comparison of DSC and DMA results, it can be said that molecular motion measured by DSC corresponds to that measured at low frequency range by DMA.

Figure 16 shows TG and DTG curves of CAPCL's with various CL/OH ratios. The samples with a low CL/OH ratio from 0 to 5 mol mol^{-1}decompose in one stage and peak temperature of DTG is observed at ca. 375°C. When the CL/OH ratio exceeds 8 mol mol^{-1}, two peaks can be observed at 375–380 and 420–425°C. Mass residue

[(m_T/m_{20})100] at 450°C, where m_t is mass at T °C and m_{20} mass at 20°C, decreased from 14 to 3% with increasing CL/OH ratio, although they are not shown in the figure.

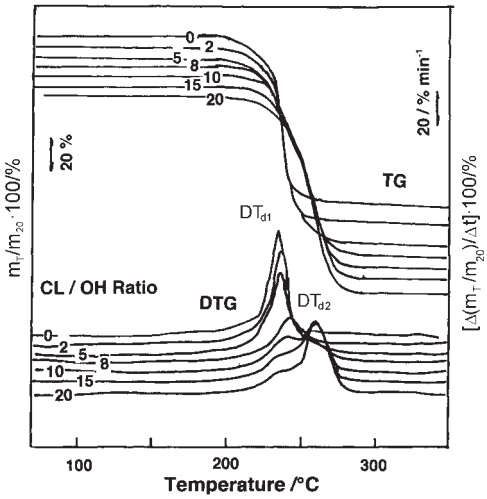

Fig. 16 TG and DTG curves of CAPCL's with various CL/OH ratios curves of CAPCL with various CL/OH ratios TG and DTG curves of CAPCL with various CL/OH ratios

As can be seen from DTG curves shown in Fig. 16, the low temperature peak (DT_{d1}) maintains almost constant value with increasing CL/OH ratio. The high temperature peak (DT_{d2}) is almost constant as shown in the figure. At the same time, the height of DTG of the low temperature side peak markedly decreased at CL/OH ratio below 8. Temperature where the mass residue reaches 50% shows similar behavior to that of DT_{d2}.

Figure 17 shows the relationship between T_d and CL/OH ratio in CAPCL's. This figure clearly shows that the thermal degradation of CAPCL's proceeds in 2 steps: degradation at lower temperature observed at around 350°C and that observed at

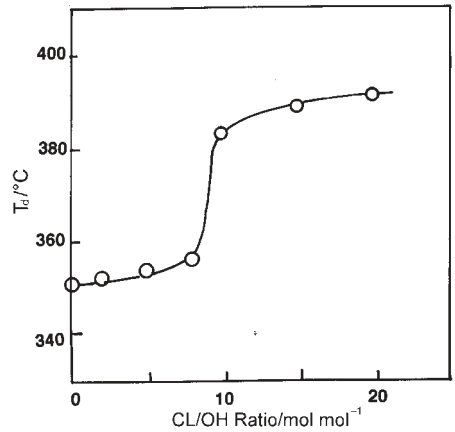

Fig. 17 Relationship between T_d and CL/OH ratio in CAPCL

higher temperature observed at around 390°C. This result strongly suggests that the 2-step thermal degradation of CAPCL's is probably caused by two chemically different structures.

Figure 18 shows a representative stacked three-dimensional diagram showing the relationship between IR intensity, wavenumber and temperature in TG-FTIR of CAPCL with CL/OH ratio 2 mol mol^{-1}. Wavenumber ranges from 600 to 4000 cm^{-1} and temperature ranges from 40 to 600°C. As shown in the diagram, IR absorption bands can mainly be observed in the temperature range from 250 to 450°C. The main peaks observed for the samples are as follows: wavenumber (assignment): 1160 cm^{-1} (νC–O–), 1260 cm^{-1} (–C(=O)–O–C–), 1517 and 1617 cm^{-1} (νC=C), 1770 cm^{-1} (νC=O), 2345 cm^{-1} (νCO_2), 2945 cm^{-1} (νC–H) and 3700 cm^{-1} (νOH).

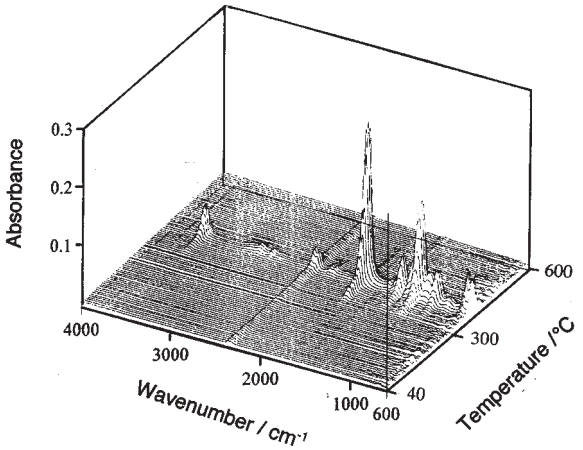

Fig. 18 Stacked three-dimensional TG-FTIR diagram for CAPCL (CL/OH ratio=2 mol mol^{-1}

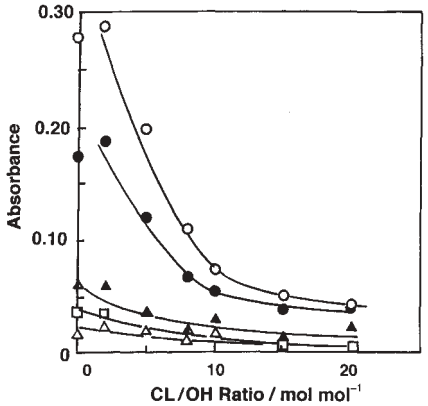

Fig. 19 Relationship between IR peak intensity corresponding to C–O–C, C=O, CO_2, CH, OH bands and CL/OH ratio in CAPCL at 380°C; ● – C–O–C, o – C=O, □ – CO_2, △ – CH, ▲ – OH

Figures 19 and 20 show the changes of C–O–C, C=O, CO_2, CH, and OH peak intensities with CH/OH ratios in CAPCL's at 380 and 430°C, corresponding to the temperatures where DT_{d1} and DT_{d2} are observed, as shown in Fig. 16. Figure 19 shows that the changes of the peak intensities corresponding to C–O–C, C=O and OH absorption peak at 380°C decrease with increasing CL/OH ratios, suggesting that the evolved gases are mainly formed by the degradation of the cellulose acetate part of CAPCL's. As shown in Fig. 20, at 430°C, the intensities of the C–O–C, C=O, CH and OH absorption peaks increase with increasing CL/OH ratios. This indicates that the evolved gases with the above groups are formed by the thermal degradation of PCL chains, since the intensities of the C–O–C, C=O and CH absorption peaks, which correspond to the structure of PCL chain, increase markedly with increasing CL/OH ratios.

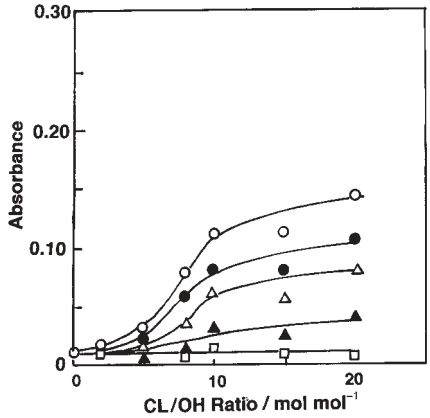

Fig. 20 Relationship between IR peak intensity corresponding to C–O–C, C=O, CO_2, CH, OH bands and CL/OH ratio in CAPCL at 430°; ● – C–O–C, o – C=O, □ – CO_2, △ – CH, ▲ – OH

The results shown in Figs 18, 19 and 20 suggest that the degradation that occurred at around 380°C corresponds to that of the cellulose acetate structure in CAPCL, and the degradation that occurred at around 430°C corresponds to that of the PCL chain.

Cellulose-based PCL's

As shown in Fig. 4, the chemical structure of CellPCL is different from that of CAPCL, since each OH group at the glucose unit of cellulose is almost converted to PCL chain. On the other hand, CAPCL shown in Fig. 3 has about one PCL chain per each cellobiose unit of the cellulose chain.

Figure 21 shows stacked DSC heating curves of CellPCL's measured at 10°C min^{-1}. As shown in Fig. 21, a baseline deviation showing glass transition is not observed for the cellulose sample (shown as CL/OH ratio=0), while T_g's for CellPCL's are clearly observed. CellPCL's with CL/OH ratios=0.33 and 0.66 show T_{g2} at around 150°C except T_{g1}. T_{g2} is considered to be related with the main chain motion of cellulose backbone of

CellPCL, since this motion was also observed in the case of CAPCL as mentioned in chapter 'Cellulose acetate-based PCL derivatives'. T_{g1}'s are observable when CL/OH ratios are between 0.3 and 5. However, T_g becomes difficult to be observed when the increasing CL/OH ratio is over 6, since the influence of PCL side chain becomes large and endothermic peaks caused by melting of PCL (T_m) makes it difficult to detect the baseline deviation caused by glass transition.

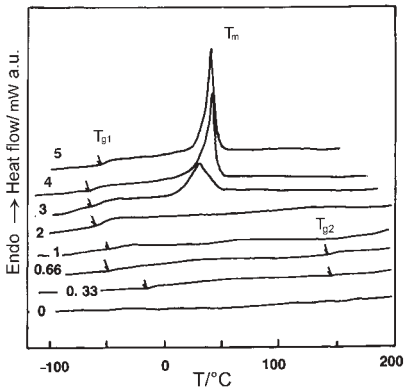

Fig. 21 DSC heating curves of CellPCL

Figure 22 shows relationship between T_g's and CL/OH ratio. As shown in Fig. 4, the numbers of PCL side chains attached to each cellobiose unit of cellulose backbone are almost 6 times that of CAPCL (Fig. 3). Accordingly, it may be reasonable to consider that CellPCL shown in Fig. 22 shows T_g's similar to that of CAPCL shown in Fig. 11, although CL/OH ratio of CellPCL is far lower than that of CAPCL.

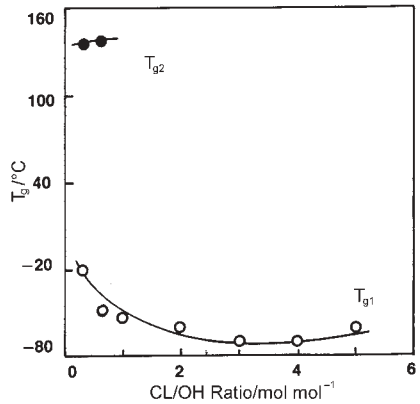

Fig. 22 Relationship between T_g and CL/OH ratio in CellPCL; o – T_{g1}, ● – T_{g2}

As mentioned in chapter 'Cellulose acetate-based PCL derivatives', the results shown in Fig. 22 are reasonable if T_g becomes observable when intermolecular distance expands by the introduction of large side chain molecules such as PCL and

when the geometrical free space enhances the main chain motion of the main chain. T_g of PCL decreases in the initial stage when CL/OH ratio is low and increases slightly after reaching a minimum point at around CL/OH=3 mol mol^{-1}. The T_g increase observed in the sample with CL/OH ratio over 3 suggests that the molecular motion of PCL random chains is restricted by the presence of the crystalline region. When the numbers of PCL chains are sufficiently large, the effect of the ordered arrangement of PCL chains on the molecular motion becomes marked, even if the chain length of each PCL chain is short (Fig. 11).

As shown in Fig. 21, the melting peak of PCL chains is observed for the PCL samples with CL/OH ratio 3, 4 and 5 mol mol^{-1}. An endothermic peak observed at around 50°C is attributable to the melting of PCL chains, and is explained by the observation in chapter 'Cellulose acetate-based PCL derivatives'.

Figure 23 shows the relationships between T_m, ΔH_m and CL/OH ratio. T_m and ΔH_m increase with increasing CL/OH ratio. It is noteworthy that T_m and ΔH_m values almost level off when CL/OH ratio becomes 5. This result strongly suggests that large numbers of PCL chains attached to the cellulose backbone have a strong influence on the molecular arrangement of CellPCL compared with that of CAPCL, since the numbers of PCL side chains attached to each cellobiose unit in CellPCL is far larger than those attached to the acetylated cellobiose unit of CAPCL.

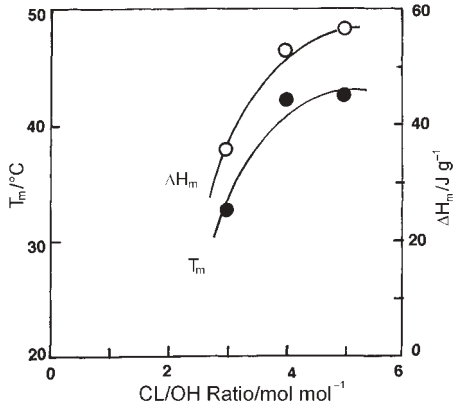

Fig. 23 Relationship between T_m, ΔH_m and CL/OH ratio in CellPCL; ● – T_m, o – ΔH_m

Figure 24 shows TG and DTG curves of CellPCL's with various CL/OH ratios from 0 to 5. The samples with a low CL/OH ratio from 0 to 1 mol mol^{-1} decompose in one stage and the peak temperature of DTG (DT_{d1}) increases from ca 340 to 360°C. When the CL/OH ratio exceeds 2 mol mol^{-1}, the DTG peak (DT_{d2}) is observed in the temperature range between ca 380 and 420°C. However, as shown in Fig. 25, T_d did not show clearly 2-step thermal degradation as was shown in Fig. 17.

Figure 26 shows a representative stacked three-dimensional diagram showing the relationship between IR intensity, wavenumber and temperature in TG-FTIR of CellPCL with CL/OH ratio 4 mol mol^{-1}. Wavenumber ranges from 600 to 4000 and temperature ranges from 40 to 600°C. As shown in the diagram, IR absorption bands

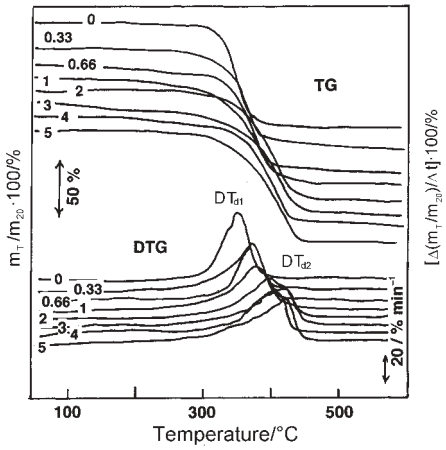

Fig. 24 TG and DTG curves of CellPCL with various CL/OH ratios

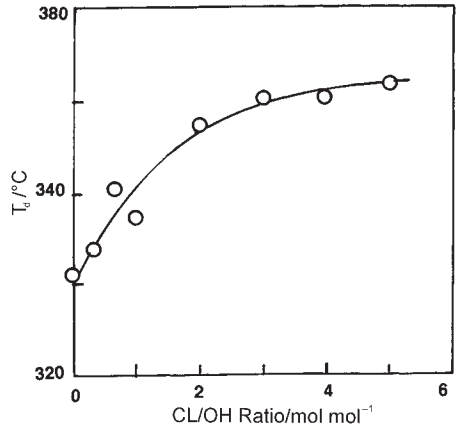

Fig. 25 Relationship between T_d and CL/OH ratio in CellPCL

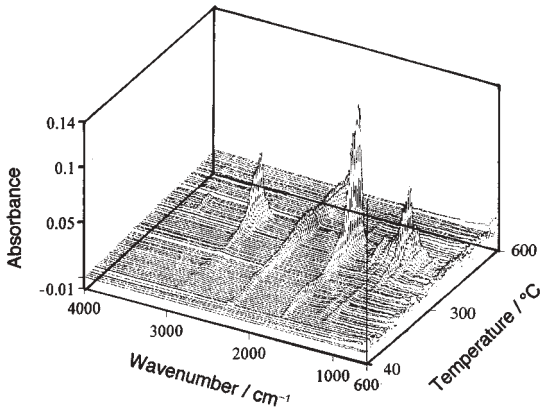

Fig. 26 Stacked TG-FTIR curves of CellPCL (CL/OH ratio=4 mol mol^{-1})

are observed in the temperature range from 300 to 450°C. The main peaks observed for the samples are almost similar to those shown in Fig. 18.

Figure 27 shows FTIR spectra at 370 and 430°C for CellPCL with CL/OH ratio 4 mol mol^{-1}. The assignments for the peaks are indicated in Fig. 27. It is seen that the intensities of absorption peaks change according to the degradation temperature of the samples. At 370°C, the IR absorption intensities of each peak are lower than those at 430°C, showing that the degradation of CellPCL at 370°C is less than that at 430°C.

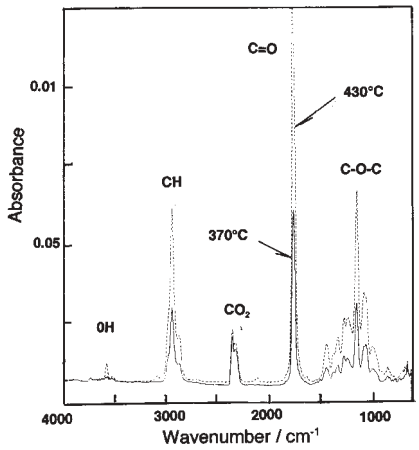

Fig. 27 TG-FTIR of CellPCL (CL/OH ratio=4 mol mol^{-1}); —– 370°C, --- – 430°C

Figures 28 and 29 show the changes of C–O–C, C=O, CO_2, CH, and OH peak intensities with CH/OH ratios in CellPCL's at 370 and 430°C, corresponding to the temperatures shown in Fig. 27. Figure 28 shows that the change of the peak intensities corresponding to C–O–C, C=O, and CH absorption peaks at 370°C slightly increase with increasing CL/OH ratios. As shown in Fig. 29, at 430°C, the intensities of

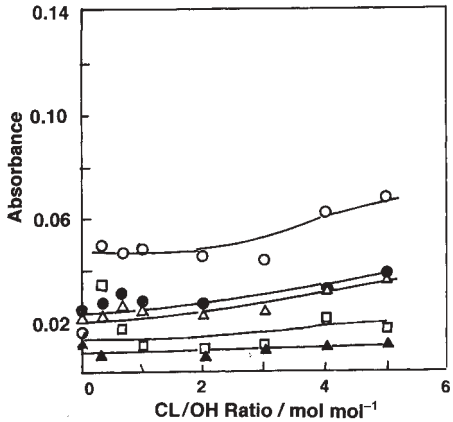

Fig. 28 Relationship between IR peak intensity corresponding to C–O–C, C=O, CO_2, CH, OH bands and CL/OH ratio in CellPCL at 370°C; ● – C–O–C, o – C=O, □ – CO_2, △ – CH, ▲ – OH

the C–O–C, C=O, CH, CO_2 and OH absorption peaks increase with increasing CL/OH ratios. In particular, the peak intensity corresponding to the C–O–C, C=O, and CH absorption increases prominently with increasing CL/OH ratios.

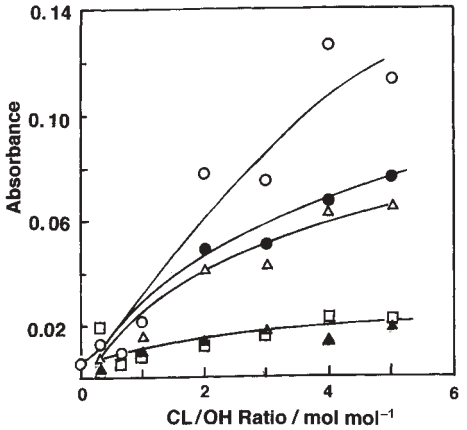

Fig. 29 Relationship between IR peak intensity corresponding to C–O–C, C=O, CO_2, CH, OH bands and CL/OH ratio in CellPCL at 430°C; ● – C–O–C, o – C=O, □ – CO_2, △ – CH, ▲ – OH

In comparison with the results described in chapter 'Cellulose acetate-based PCL derivatives', it can be said that the above results shown in Figs 27, 28 and 29 suggest that the degradation that occurred at around 370°C corresponds to that of the cellulose structure in CellPCL, and that the degradation that occurred at around 430°C corresponds to that of the PCL chain.

Lignin-based PCL's

Figure 30 shows part of the stacked magnified DSC heating curves of KL based PCL (KLPCL) with various CL/OH ratios from 2 to 25 mol mol^{-1} measured in the temperature range from –100 to 150°C. A marked change in baseline due to glass transition was ob-

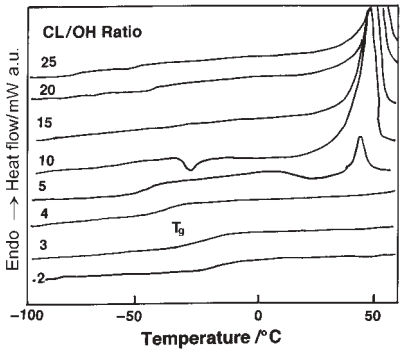

Fig. 30 Stacked magnified DSC heating curves of KLPCL with various CL/OH ratios

served in each DSC curve. T_g's were determined by the method reported previously [31, 37]. T_g decreases with increasing CL/OH ratio from 2 to 10 mol mol^{-1} in KLPCL's , since PCL chains with lignin act as soft segments in KLPCL molecular networks. However, as shown in Fig. 30, when the CL/OH ratio is 10 to 25 mol mol^{-1}, T_g increases. In the case of the DSC curves representing KLPCL's with CL/OH ratio 10 mol mol^{-1}, a prominent exothermic peak due to cold-crystallization of KLPCL and also a recognizable peak due to melting of crystals are observed when CL/OH ratio is over 10 mol mol^{-1}. The above results suggest that KLPCL's with CL/OH ratios over 10 mol mol^{-1} have a clear crystalline region in the molecular structure. A similar phenomenon was observed in ALPCL's.

Figure 31 shows a phase diagram of KLPCL according to the above results. In general, no large difference is observed between T_g and T_m of KLPCL and those of ALPCL.

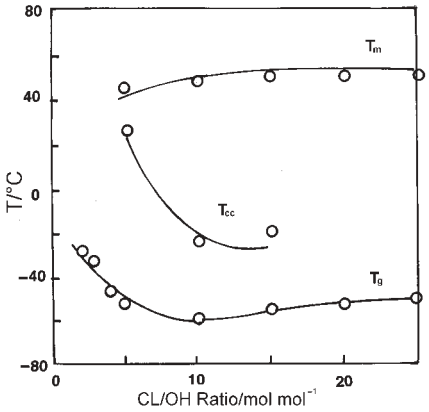

Fig. 31 Phase diagram of KLPCL

Figure 32 shows the changes of T_g's of AL- and KLPCL's. The T_g decreases markedly with increasing CL/OH ratio in the region where CL/OH ratio is below 10 mol mol^{-1} and then the T_g increases with increasing CL/OH ratio in the region

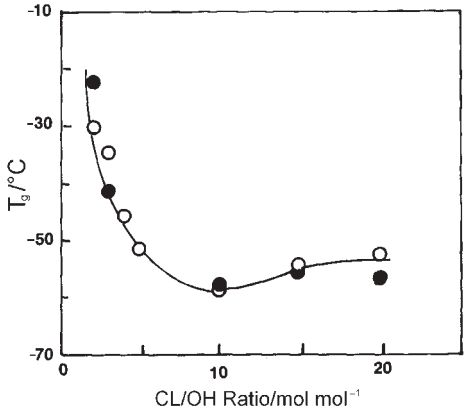

Fig. 32 Relationship between T_g and CL/OH ratio for AL- and KLPCL's; ● – ALPCL, o – KLPCL

where CL/OH ratio exceeds 10 mol mol^{-1}. The increase of T_g over CL/OH ratio=10 mol mol^{-1} suggests that by the introduction of long PCL chains, the crystalline region increased and that this restricted the motion of PCL chains in both AL- and KLPCL's. As the above facts strongly suggest, the effect of structural difference between AL and KL does not affect markedly the phase transition of AL- and KLPCL's, suggesting that both lignins are available as good raw materials for the preparation of PCL derivatives.

Figure 33 shows TG and DTG curves of KLPCL's with CL/OH ratios of 2, 5 and 25 mol mol^{-1}. Similar TG and DTG curves of ALPCL's were also obtained. It is clearly seen from DTG curves that samples start to decompose at around 300°C. It is also seen from the DTG curves that samples with low values of CL/OH ratios (CL/OH ratio=2 and 5 mol mol^{-1}) decompose in multiple steps in the temperature range from 300 to 450°C, since DTG peaks are broad and show tailing to the low temperature side. However, the DTG curve for KLPCL with CL/OH ratio 25 mol mol^{-1} shows an apparently narrow curve without tailing. Therefore, it can be said that the thermal degradation of PCL with lower values of CL/OH ratios is probably affected by thermal degradation of the lignin core structure in KLPCL derivatives.

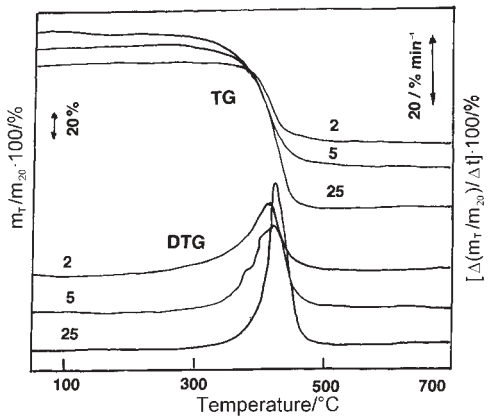

Fig. 33 TG and DTG curves of KLPCL's with CL/OH ratios of 2, 5 and 25

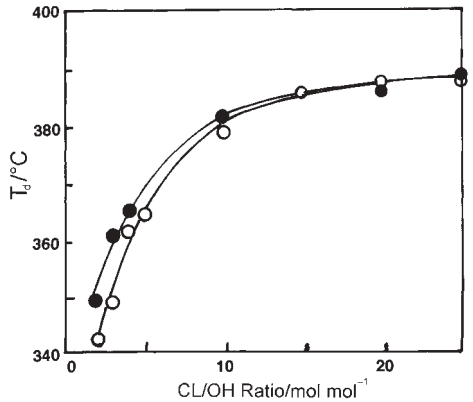

Fig. 34 Relationship between T_d and CL/OH ratio for AL- and KLPCL's; ● – ALPCL, o – KLPCL

Figure 34 shows the relationship between T_d and CL/OH ratio for AL- and KLPCL's. T_d initially increases and then levels off with increasing CL/OH ratio over 10 mol mol^{-1}. We have reported that lignin becomes thermally stable when OH groups of lignin are methylated and acetylated [38], since reactive OH groups are blocked. Accordingly, the increase in T_d values of AL- and KLPCL's can be attributed to the introduction of PCL chains to the OH group of lignins.

Figure 35 shows a representative TG-FTIR stacked three-dimensional diagram showing the relationship between IR intensity, wavenumber and temperature in TG-FTIR of KLCL with CL/OH ratio 10 mol mol^{-1}. The assignment of the main peaks observed for the sample are almost the same as described in chapter 'Cellulose acetate-based PCL derivatives': i.e. 1160 cm^{-1} (νC–O–), 1260 cm^{-1} (–C(=O)–O–C–), 1517 and 1617 cm^{-1} (νC=C), 1770 cm^{-1} (νC=O), 2345 cm^{-1} (νCO$_2$), 2945 cm^{-1} (νC–H) and 3700 cm^{-1} (νOH).

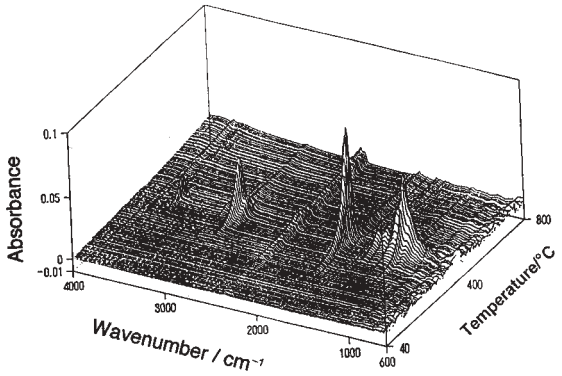

Fig. 35 Stacked three-dimensional TG-FTIR diagram for KLPCL (CL/OH ratio=10 mol mol^{-1})

Figures 36 and 37 show the changes of C–O–C, C=O, CO_2 , CH, and OH peak intensities with CH/OH ratios in KLPCL's at 380 and 420°C. Figure 36 shows that

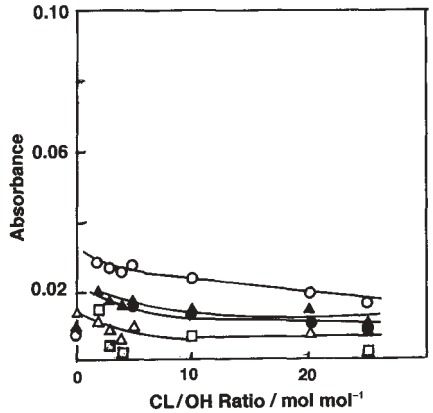

Fig. 36 Changes of C–O–C, C=O, CO_2, CH, and OH peak intensities with CH/OH ratios in KLPCL's at 380°C; ● – C–O–C, o – C=O, □ – CO_2, △ – CH, ▲ – OH

the change of the peak intensities corresponding to the above IR absorption peaks at 380°C decrease slightly with increasing CL/OH ratios, suggesting that the evolved gases are not prominently formed at this temperature range. As shown in Fig. 37, at 420°C, the intensities of the C–O–C, C=O, CH and OH absorption peaks increase recognizably with increasing CL/OH ratios. This indicates that KLPCL degrades considerably and that the evolved gases with the above groups are formed by the thermal degradation of PCL chains, since the intensities of the C–O–C, C=O and CH absorption peaks, which correspond to the structure of PCL chain, increase prominently with increasing CL/OH ratios.

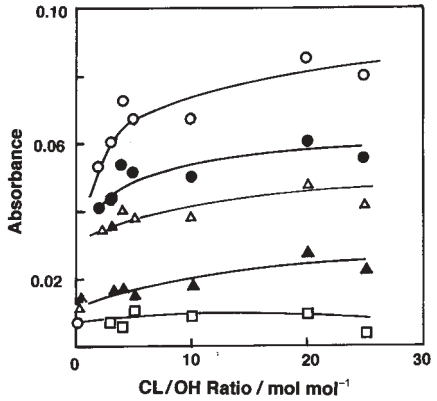

Fig. 37 Changes of C–O–C, C=O, CO_2, CH, and OH peak intensities with CH/OH ratios in KLPCL's at 420°C; ● – C–O–C, o – C=O, □ – CO_2, △ – CH, ▲ – OH

Figure 38 shows the changes of C=O peak intensity with various CH/OH ratios in KLPCL at 380, 400, 420, 430 and 440°C. The peak intensity of C=O peak at 380 and 400°C decreases with increasing CL/OH ratios, suggesting that the evolved gases are not formed by the degradation of PCL chains but mainly formed by the degradation of lignin in KLPCL. The C=O peak intensity increases recognizably in the temperature range over

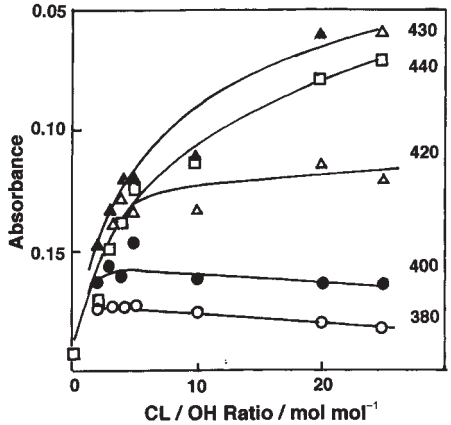

Fig. 38 Changes of C=O peak intensity with CL/OH ratio in KLPCL at various temperatures (°C)

420°C. This peak intensity also increases prominently with increasing CL/OH ratio. The above results indicate that the evolved gas with C=O group is formed by the thermal degradation of PCL chains. The intensity of the C=O peak at 430°C is larger than that at 440°C. This may suggest that the evolution of gases caused by PCL chain occurs most prominently in the temperature range around 430°C.

Saccharide-based PU's

It is generally recognized that polyurethane (PU) is one of the most useful three-dimensional polymers, since PU has unique features: for example, various forms of materials such as sheets, foams, adhesives and paints can be obtained from PU, and their physical properties can easily be controlled.

Figure 39 shows DSC curves obtained for fructose-based PU samples. The base line shifts due to the glass transition are clearly seen in the figure.

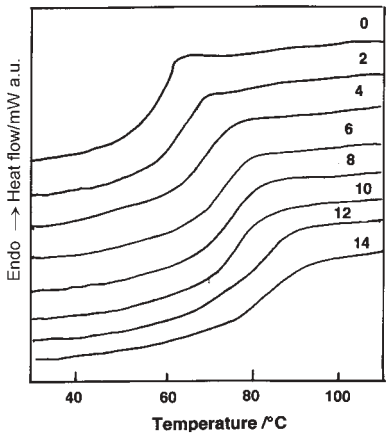

Fig. 39 DSC curves obtained for PU samples from fructose. Numbers in figure shows fructose contents (%) in PEG

Figure 40 shows the relationship between T_g and the saccharide content. T_g increased steadily with the saccharide content for all PU's from glucose, fructose and su-

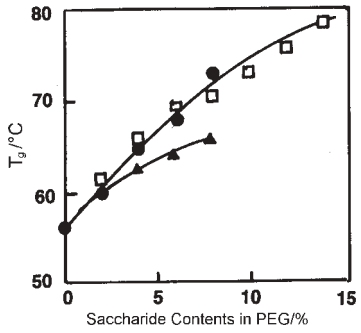

Fig. 40 Relationship between T_g and saccharide content ; ● – glucose, □ – fructose, ▲ – sucrose

crose. The incorporation of saccharides into the PU structure leads to an increase in crosslinking density due to the large number of hydroxyl groups per molecule for the saccharides. The number of hydroxyl groups per molecule of glucose and fructose is 5 mol mol^{-1} and sucrose has a number of hydroxyl groups per molecule of 8 mol mol^{-1}. The higher the crosslinking density, the more restricted is the main chain motion and the higher is T_g. In addition to having a large effect on the crosslinking density, the saccharides also act as hard segments that cause an increase in T_g. As stated in chapter 'Polyurethane (PU) derivatives', the MDI content increased with the saccharide content since the NCO/OH ratio was kept constant. MDI with its benzene rings acts as hard segments and thus an increase in the MDI content results in an increment in T_g.

As shown in Fig. 40, the sucrose-containing PU's have lower T_g's than the other samples. Since sucrose contains fewer OH groups per unit of mass than glucose and fructose, the sucrose PU's have lower crosslinking. Also, since the NCO/OH ratio was kept constant, the sucrose PU's have higher PEG content and lower MDI content than the corresponding glucose- and fructose-based PU's.

Figure 41 shows the change of T_g with MP (molasses polyol) content for a flexible type PU foam which was prepared according to the process described in chapter 'Molasses-based PU foams'. As stated above, physical properties such as T_g and Young's modulus can be controlled by changing the components of PU. In the case of the flexible PU foam, as shown in Fig. 41, T_g is very low compared with that of rigid type PU's. For example, T_g's shown in Fig. 40 are between 55 and 80°C, while T_g's shown in Fig. 41 are between –55 and –50°C. The saccharide content of both PU's are almost the same, although the expression of the *x*-axis is different, since MP contains 33% of molasses in PEG. This large difference in T_g was achieved by the introduction of PPG3000 which has a long molecular chain and TDI having a lower aromatic ring content compared with MDI.

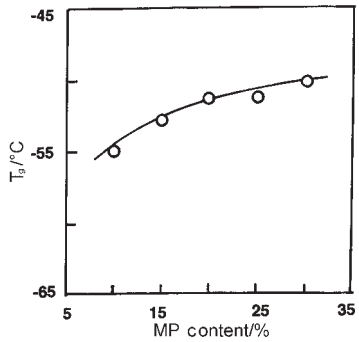

Fig. 41 Change of T_g with *MP* content in PU foams; *MP*: (mass of molasses, g/mass of PEG, g)100

Figure 42 shows DSC curves of PU's from the PE–PPG–MP–(TDI/MDI) system with various TDI/MDI ratios. As shown in Fig. 43, T_g has changed from ca –26 to –18°C by only altering the TDI/MDI ratio. This result suggests the considerable effect of the aromatic rings contained in isocyanate compounds in controlling the rigidity of PU molecules derived from saccharides.

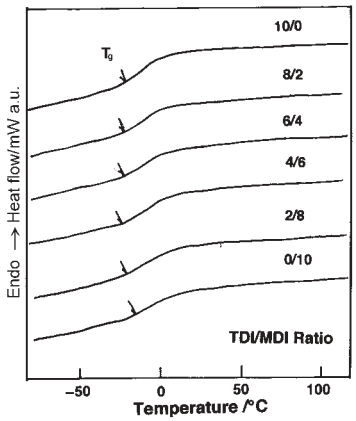

Fig. 42 DSC curves of PU's from the PE-PPG-MP-(TDI/MDI) system with various TDI/MDI ratios; Arrows indicate T_g's

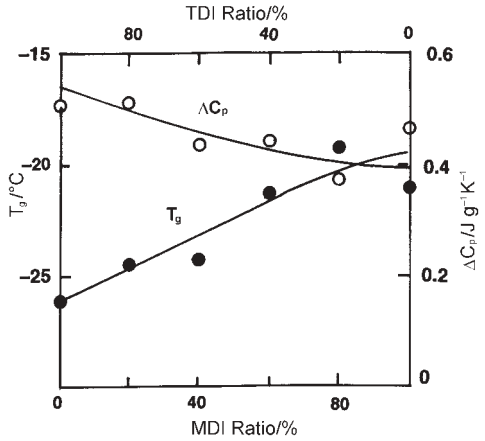

Fig. 43 Relationship between T_g, ΔC_p and MDI/TDI ratios of PU's from PE–PPG–MP–(TDI/MDI) system; ● – T_g, o – ΔC_p

Lignin-based PU's

Lignin is most useful as a raw material for the preparation of rigid type PU foams and sheets. Concerning rigid type PU sheets, their preparation and physical properties have already been reported elsewhere [39]. Accordingly, the recent development of rigid PU foams is discussed here.

Figure 44 shows the relationship between T_g's of lignin-based PU's and the contents of various lignins such as AL, KL and LS dissolved in PEG 200 in order to prepare the above PU's. As shown in Fig. 44, T_g increases with increasing lignin contents, since phenyl groups in lignin act as hard segments in PU networks regardless of the kind of lignin.

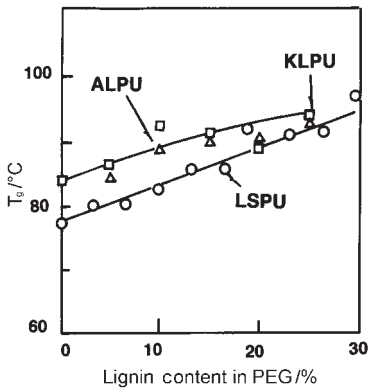

Fig. 44 Relationship between T_g's of lignin-based PU's and contents of various lignins such as AL, KL and LS; △ – ALPU, □ – KLPU, o – LSPU

As shown in Fig. 45, T_d of lignin-based PU foams prepared from AL, KL and LS decreases slightly with lignin contents. Usually the dissociation of urethane bonds between isocyanate groups and phenolic hydroxyl groups occurs in the temperature range lower than that of urethane bonds between isocyanate groups and alcoholic hydroxyl groups [18]. Accordingly, the increase of lignin content in polyol seems to result in the slight decrease of T_d of lignin-based PU foams.

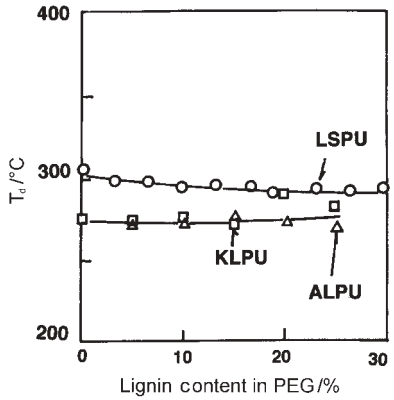

Fig. 45 Relationship between T_d of lignin-based PU foams and contents of lignins in polyol; △ – ALPU, □ – KLPU, o – LSPU

As shown in Fig. 46, the mass residue (*MR*) of lignin-based PU foams increases slightly with increasing lignin contents in polyols. This increase of *MR* is probably caused by the condensation reaction of lignin molecules which proceed with the thermal degradation of lignin [41].

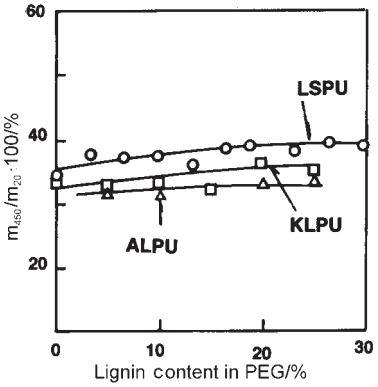

Fig. 46 *MR* of lignin-based PU foam and contents of lignins in polyol; △ – ALPU, □ – KLPU, o – LSPU

PU's derived from saccharide-based PCL's

Figure 47 shows DSC curves of PU sheets derived from Glu-PCL with various CL/OH ratios from 1 to 5 mol mol^{-1}. A marked change in baseline due to glass transition was observed in each DSC curve. Glass transition temperatures (T_g's) were determined by the method reported previously [31, 37]. T_g decreases with increasing CL/OH ratio in PU's, since caprolactone chains with saccharides act as soft segments in PU networks. This softening effect of caprolactone chains was enhanced progressively with increasing chain length of CL chains.

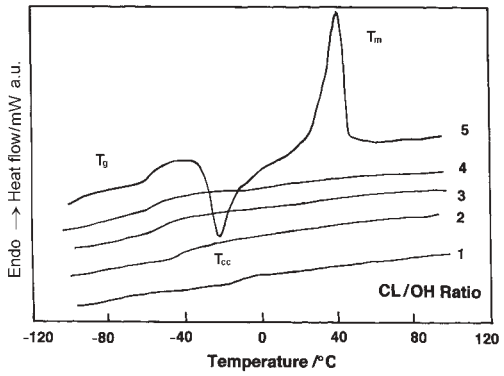

Fig. 47 DSC heating curves of PU sheets derived from Glu-PCL with various CL/OH ratios

In the case of the DSC curve representing Glu-PCL PU with CL/OH ratio 5, a recognizable exothermic peak due to cold crystallization of Glu-PCL and also a marked peak of melting of crystalline region are observed at around –20 and 40°C, respectively. The magnified DSC curve representing Glu-PCL with CL/OH ratio 4, which was annealed at room temperature, also showed a melting peak around 40°C.

The other PU's derived from Fru- and Suc-PCL's showed similar DSC results. The above results suggest that the PU's derived from the saccharide-based PCL's with CL/OH ratios over 4 have a crystalline region in the molecular structure.

Figure 48 shows the relationship between T_g's and CL/OH ratios of saccharide-based PCL in PU's. T_g decreased steadily with the CL content for all three types of PU's derived from glucose-, fructose- and sucrose-based PCL's. This can be attributed to a number of factors. The incorporation of saccharide-based PCL's into the PU structure leads to the enhancement of molecular motion of PU networks due to the flexible PCL chains attached to saccharides. The hydroxyl groups of glucose and fructose are 5 mol mol^{-1} and sucrose has 8 hydroxyl groups/each molecule. If the PCL chain in PU becomes longer, the PU molecules become more flexible in the main chain motion and lower in the T_g. In addition, the structure of the saccharide which forms the core structure affects T_g's. Accordingly, the tendency of the decrease of T_g's is different between the PU's derived from Glu- and Fru-PCL and those derived from Suc-PCL. Suc-PCL PU's show lower T_g's than those of Glu- and Fru-PU's when CL/OH ratio is low.

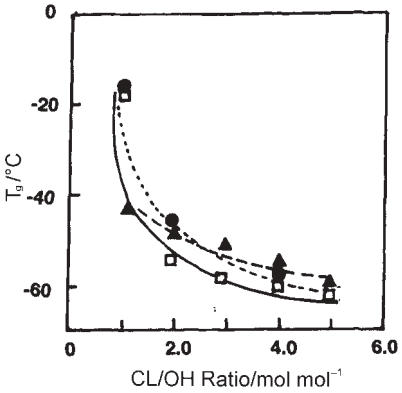

Fig. 48 Relationship between T_g's and CL/OH ratios of saccharide-based PCL's in PU's; ● – Glu-PCL PU, □ – Fru-PCL PU, ▲ – Suc-PCL PU

Figure 49 shows TG and derivative TG (DTG) curves of PU's with various CL/OH ratios derived from Suc-PCL PU's with CL/OH ratios, 1, 3 and 5 mol mol^{-1} measured in N_2. In the TG curves of PU's a small mass change is observed at around 100°C, which can be attributed to the evaporation of water from the samples. At a temperature higher than 500°C, mass residues are observed in TG curves. As seen in Fig. 49, the thermal decomposition occurred in almost a single step until a certain temperature (up to ca 420°C). This suggests that the degradation process occurring up to this temperature region can mainly be attributed to the dissociation of urethane linkages between hydroxyl groups of PCL and isocyanate groups.

As shown in Fig. 50, T_d's of PU's increased from ca 320 to 380°C with increasing CL/OH ratio. From this result, it is considered that the dissociation of the urethane linkage formed between the isocyanate group and the OH group of PCL with increased chain length seems to occur with more difficulty than that formed between the isocyanate group and the OH group of saccharides.

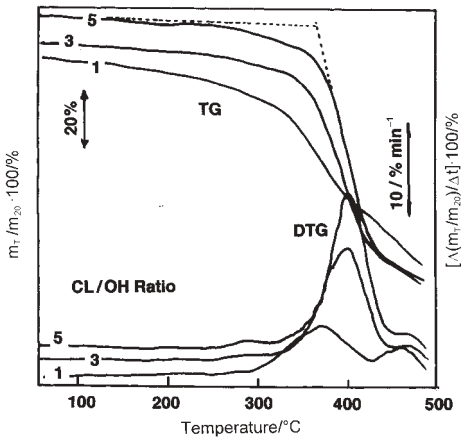

Fig. 49 TG and derivative TG (DTG) curves of saccharide-based PCL PU's with various CL/OH ratios

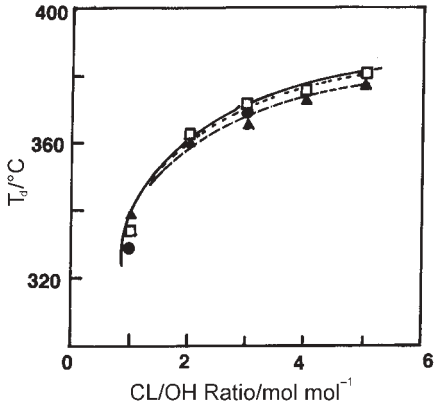

Fig. 50 Relationship between T_d's of PU's and various CL/OH ratios of saccharides; ● – Glu-PCL PU, □ – Fru-PCL PU, ▲ – Suc-PCL PU

Figure 51 shows the relationship between the mass residue and the CL/OH ratios in PU's derived from saccharide-based PCL's. There appears to be almost a linear relationship between the residue at 450°C and the CL/OH ratio, suggesting that the saccharides constitute a significant part of the residual products. This indicates that the thermal decomposition of these PU's is to a fairly large extent caused by the dissociation of isocyanate groups and hydroxyl groups of PCL.

PU's derived from lignin-based PCL's

Figure 52 shows magnified DSC curves of PU's derived from KLPCL with various CL/OH ratios from 2 to 25 mol mol^{-1}. A marked change in baseline due to glass transition was observed in each DSC curve. T_g decreases with increasing CL/OH ratio from 2 to 10 mol mol^{-1} in PU's from Lig-PCL's. PCL chains with lignin act as soft

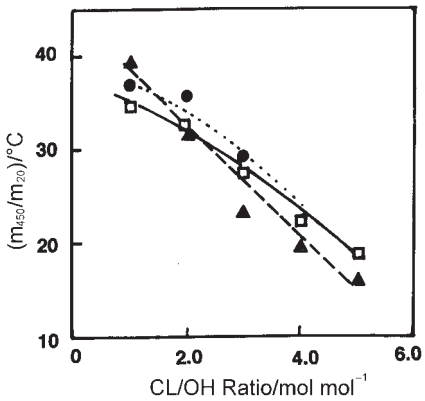

Fig. 51 Relationship between the mass residue and the CL/OH ratios;
● – Glu-PCL PU, □ – Fru-PCL PU, ▲ – Suc-PCL PU

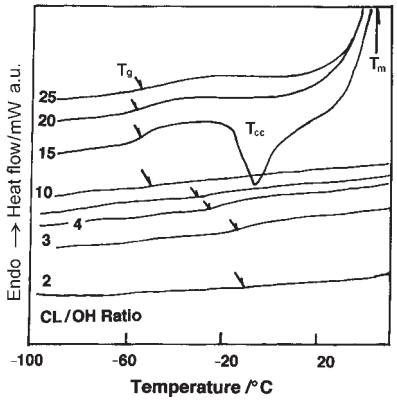

Fig. 52 Magnified DSC heating curves of PU's derived from KLPCL

segments in PU networks. However, as shown in Fig. 52, when the CL/OH ratio is 10 to 25 mol mol^{-1}, T_g increased. In the case of the DSC curves representing KLPCL PU with CL/OH ratio 15 mol mol^{-1}, an exothermic peak due to cold-crystallization of KLPCL PU and also a large peak due to the melting of crystalline region are observed when CL/OH ratio is over 15. The above results suggest that the PU's derived from KLPCL's with CL/OH ratios over 15 have a clear crystalline region in the molecular structure. A similar phenomenon was observed in PU's from ALPCL's.

Figure 53 shows the changes of T_g's of PU's from AL- and KLPCL's. The T_g markedly decreases with increasing CL/OH ratio in the region where CL/OH ratio below 15 mol mol^{-1} and then the T_g levels off with increasing CL/OH ratio in the region where CL/OH ratio exceeds 15. The leveling off of T_g over CL/OH ratio= 15 mol mol^{-1} suggests that by the introduction of long PCL chains the crystalline region increased and this restricted the motion of PCL chains.

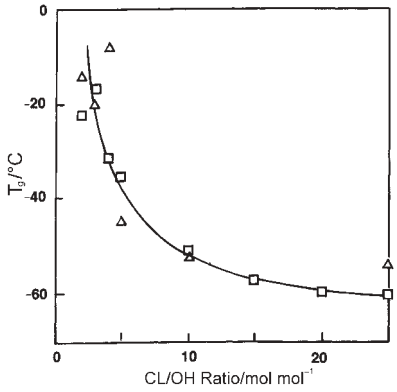

Fig. 53 Changes of T_g's of PU's derived from AL- and KLPCL's; △ – ALPCL PU, □ – KLPCL PU

Figure 54 shows the changes of T_g's, cold-crystallization temperatures (T_{cc}'s) and melting temperatures (T_m's), *vs*. CL/OH ratios of PU's derived from AL- and KLPCL's. The change of T_g's is almost the same for the AL- and KLPCL PU's. T_{cc}'s and T_m's slightly increase with increasing CL/OH ratio in the region over CL/OH ratios over 15, suggesting the increase in the crystalline region of PCL chains in the AL- and KLPCL PU's.

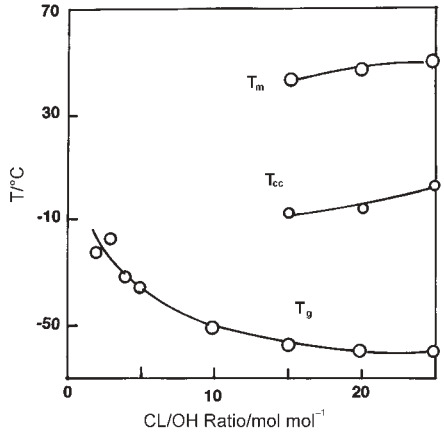

Fig. 54 Phase diagram of PU's derived from KLPCL with various CL/OH ratios

TG and DTG curves of PU's derived from lignin-based PCL's with various CL/OH ratios showed two kinds of thermal degradation temperatures, T_{d1} and T_{d2} [42].

Figure 55 shows the change of T_{d1} and T_{d2} with CL/OH ratios of AL- and KLPCL PU's. Matsuzak and Frisch reported that some urethane bonds in PU's dissociate to form hydroxyl and isocyanate groups at about 200°C [43]. Domberg *et al*. proposed a mechanism where a dehydration reaction of hydroxyl groups in alkyl groups and heterolysis and homolysis dissociation of β-aryl ether bonds in lignin occur initially

at about 200°C [44, 45]. Accordingly, it is considered that T_{d1} may reflect the degradation of lignin parts in AL- and KLPCL PU's. As shown in Fig. 17, T_d of CAPCL increased suddenly and stepped up from 350 to 390°C with increasing CL/OH ratio from that lower than 8 to that higher than 10. The above change of T_d accords well with the change of T_{d2} of KLPCL PU's as shown in Fig. 55. The change of T_{d2} of ALPCL PU's showed a similar tendency. Accordingly, it is considered that T_{d1} probably reflects the degradation of the lignin part and T_{d2} may reflect that of the PCL parts in KLPCL PU's. A similar tendency was observed in the case of ALPCL PU's.

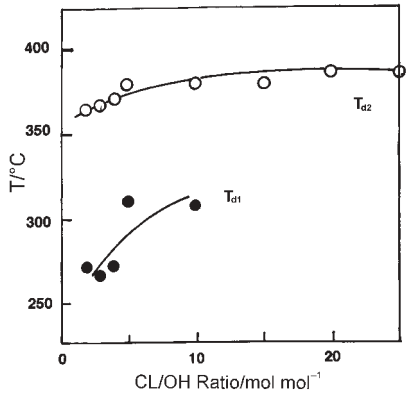

Fig. 55 Change of T_{d1} and T_{d2} with CL/OH ratios of AL- and KLPCL PU's; ● – T_{d1}, o – T_{d2}

Figure 56 shows the changes of IR absorption intensity of C–O–C, C=O, CO_2 and OH peaks of evolved gases from KLPCL PU's. ALPCL PU's also showed a similar tendency. The changes of IR absorption intensities calculated at 420°C are almost similar. The IR absorption intensity of CO_2 gas from AL- and KLPCL PU's do not show the PCL chain length dependency, while the other IR absorption peaks show the PCL chain length dependency. This suggests that the evolution of CO_2 gas occurs randomly and is not specific to the chemical structure. The IR absorption intensities

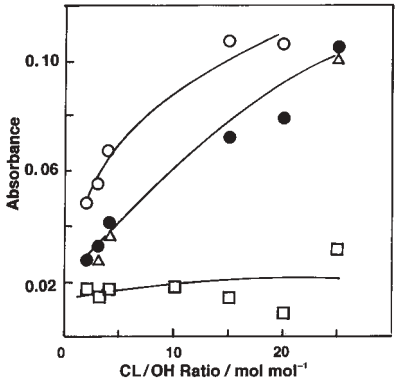

Fig. 56 Changes of IR absorption intensity of characteristic peaks of evolved gases from KLPCL PU's; ● – C–O–C, o – C=O, □ – CO_2, △ – CH

corresponding to C–O–C, C=O and CH peaks increase markedly with increasing CL/OH ratios. This suggests that gases having C–O–C, C=O and CH groups are evolved from PCL chains. The above facts also well accorded with the decrease of the mass residue with increasing PCL chain length in lignin-based PCL PU's.

Conclusions

Environmentally compatible polymers such as polycaprolactone (PCL) and polyurethane (PU) derivatives were synthesized from saccharides, polysaccharides and lignins such as glucose, fructose, sucrose, cellulose, cellulose acetate, alcoholysis lignin, Kraft lignin and sodium lignosulfonate. Polymerization was initiated by the OH group of saccharides, polysaccharides and lignins.

Saccharide- and lignin-based PCL derivatives with various PCL chain lengths were prepared. PU sheets were also prepared from the above PCL derivatives by the reaction with diphenylmethane diisocyanate (MDI). Glass transition temperatures (T_g's), cold-crystallization temperatures (T_{cc}'s) and melting temperatures (T_m's) of saccharide- and lignin-based PCL's and PU's were determined by DSC, and phase diagrams were obtained. T_g's decreased with increasing CL/OH ratio, suggesting that PCL chains act as a soft segment in the amorphous region of PU molecules. Two thermal degradation temperatures (T_d's) were observed in TG curves of PU's from saccharide- and lignin-based PCL's with low CL/OH ratios. TG-FTIR analysis of PU's from lignin-based PCL's suggested that compounds having C–O–C, C=O and C–H groups are mainly produced by thermal degradation of PCL chains in lignin-based PCL's and PU's.

Flexible and rigid PU sheets and foams were also prepared by the reaction of OH groups of saccharides and lignins with isocyanates such as TDI and MDI. The methods controlling mechanical properties such as stress and elasticity of PU's through changing thermal properties such as glass transition temperature were established. One method to control physical properties was changing molecular flexibility through the control of the length of molecular chain by similar methods as reported above for the case of PCL derivatives. Another method to control physical properties was regulating the cross-linking points in PU molecular networks.

From the above results, we may conclude that saccharides, polysaccharides and lignins can be used as very useful components of environmentally compatible polymers such as PCL's and PU's. Saccharides and lignins efficiently act as hard segments in the above polymers. It can also be concluded that the influence of the introduction of saccharide and lignin in the molecular chain of polymers such as PU's on physical properties is greater than other factors such as the NCO/OH ratio and the molecular mass of polyols such as PEG. It is possible to control the flexibility and rigidity of the prepared polymers by changing the molecular chain length that connects saccharide and lignin components in the polymer networks.

It is noteworthy that thermal analysis is a very useful and helpful characterization method in establishing the molecular design of new polymers.

The author would like to express his sincere thanks to Professor Dr. Tatsuko Hatakeyama and Professor Dr. Kunio Nakamura (Otsuma Women's University), Dr. Shigeo Hirose (National Institute of Advanced Science and Technology), Dr. Per B. Zetterlund (Osaka City University), Professor Dr. Noriyuki Morohoshi (Tokyo University of Agriculture and Technology), Professor Dr. Masato Takahashi (Shinsyu University) and Dr. Ryohei Tanaka (Japan International Research Center for Agricultural Science) for their cooperative research works.

Appendix

Symbols and abbreviations

Symbols

C_p	heat capacity
ΔC_p	heat capacity difference at T_g
ΔH_m	enthalpy of melting
E_a	activation energy
E'	dynamic storage modulus
E''	dynamic loss modulus
T_{cc}	cold-crystallization temperature
T_d	thermal degradation temperature
T_g	glass transition temperature
T_m	melting temperature
tanδ	E''/E'

Abbreviations

AL	alcoholysis lignin (Alcel lignin®)
ALPCL	alcoholysis lignin-based PCL
CA	cellulose acetate
CAPCL	cellulose acetate-based PCL
CellPCL	cellulose-base polycaprolactone derivatives
CL	ε-caprolactone
DABCO	triethylene diamine
DTDL	dibutyltin dilaurate
DEG	diethylene glycol
DSC	differential scanning calorimetry
DMA	dynamic mechanical analysis
DMAc	N,N-dimethylacetoamide
DTA	differential thermal analysis
FTIR	Fourier transform infrared spectrometry

Fru	fructose
Glu	glucose
KL	kraft lignin
KLPCL	kraft lignin-based PCL
LiCl	lithium chloride
LigPCL	lignin-based PCL
MDI	diphenylmethane diisocyanate
MP	molasses polyol
MR	mass residue
PCL	poly(ε-caprolactone)
PEG	poly(ethylene glycol)
PPG	poly(propylene glycol)
PU	polyurethane
Suc	sucrose
TDI	toluene diisocyanate
TG	thermogravimetry

References

1 H. Hatakeyama, E. Hayashi and T. Haraguchi, Polym., 18 (1977) 759.
2 T. Hatakeyama, K. Nakamura and H. Hatakeyama, Polym., 19 (1978) 593.
3 K. Nakamura, T. Hatakeyama and H. Hatakeyama, Polym. J., 15 (1983) 361.
4 S. Hirose, H. Hatakeyama and T. Hatakeyama, Sen-i Gakkaishi, 39 (1983) 496.
5 V. P. Saraf and W. G. Glasser, J. Appl. Polym. Sci., 29 (1984) 1831.
6 V. P. Saraf and W. G. Glasser, J. Appl. Polym. Sci., 30 (1985) 2207.
7 K. Nakamura, T. Hatakeyama and H. Hatakeyama, Polym. J., 18 (1986) 219.
8 H. Yoshida, R. Morck, K. P. Kringstad and H. Hatakeyama J. Appl. Polym. Sci., 34 (1987) 1187.
9 S. Hirose, S. Yano, T. Hatakeyama and H. Hatakeyama, ACS Symposium Ser. 397, ACS, Washington DC, 1989, p. 382.
10 H. Hatakeyama, S. Hirose and T. Hatakeyama, ACS Symposium Ser. 397, ACS, Washington DC, 1989, p. 205.
11 T. Hatakeyama, K. Nakamura, S. Yoshida and H. Hatakeyama, Food Hydrocolloids, 3 (1989) 301.
12 S. Hirose, K. Nakamura and T. Hatakeyama, Cellulose and Wood (Ed. C. Schuerch) John Wiley and Sons, N. Y., 1989, p. 1133.
13 R. Morck, A. Reimann, K. Kringstad and H. Hatakeyama, Wood Processing and Utilization, 21 (1989) 175.
14 H. Yoshida, R. Morck, K. P. Kringstad and H. Hatakeyama, J. Appl. Polym. Sci., 40 (1990) 1819.
15 K. Nakamura, T. Hatakeyama and H. Hatakeyama, Polym. J., 23 (1991) 253.

16 R. Morck, A. Reimann, K. P. Kringstad and H. Hatakeyama, Polym. Adv. Technol., 2 (1991) 41.
17 T. Hatakeyama and H. Hatakeyama, Viscoelasticity of Biomaterials (Eds W. G. Glasser and H. Hatakeyama), ACS Symp. Ser. 489, ACS, Washington DC 1992, p. 218.
18 S. Hirose and H. Hatakeyama, Polyphenols Actualities, 8 (1992) 13.
19 H. Hatakeyama and T. Hatakeyama, Thermochim. Acta, 308 (1998) 3.
20 R. Tanaka, T. Hatakeyama and H. Hatakeyama, Polym. Inter., 45 (1998) 118.
21 H. Hatakeyama, S. Hirose, K. Nakamura and T. Hatakeyama, Cellulosics: Chemical, Biochemical and Material Aspects, (Eds J. F. Kennedy, G. O. Phillips and P. A. Williams), Ellis Horwood, Chichester 1993, p. 524.
22 N. Morohoshi, S. Hirose, H. Hatakeyama, T. Tokashiki and K. Teruya, Sen-i Gakkaishi, 51 (1995) 143.
23 H. Hatakeyama, S. Hirose, T. Hatakeyama, K. Nakamura, K. Kobashigawa and N. Morohoshi, J. Macromol. Sci., Pure Appl. Chem., A32 (1995) 743.
24 M. J. Donnely, Polym. Inter., 37 (1995) 297.
25 K. Nakamura, Y. Nishimura, P. Zetterlund, T. Hatakeyama and H. Hatakeyama, Thermochim. Acta, 282/283 (1996) 433.
26 P. Zetterlund, S. Hirose, T. Hatakeyama, H. Hatakeyama and A-C. Albertsson, Polym. Inter., 42 (1997) 1.
27 H. Hatakeyama, K. Kobashigawa, S. Hirose and T. Hatakeyama, Macromol. Symp., 130 (1998) 127.
28 T. Hatakeyama, T. Tokashiki and H. Hatakeyama, Macromol. Symp., 130 (1998) 139.
29 A. Gandini and N. M. Belgacem, Polym. Inter., 47 (1998) 267.
30 M. Funaoka, Polym. Inter., 47 (1998) 277.
31 T. Hatakeyama and F. X. Quinn, Thermal Analysis, Fundamentals and Applications to Polymer Science, Wiley, Chichester 1994.
32 K. Kamide and M. Sato, Polym. J., 17 (1985) 919.
33 C. G. Pitt, Biodegradable Polymers and Drug Delivery Systems, (Eds M. Chasin and R. Langer), Marcel Dekker Inc. New York 1990, p. 81.
34 E. J. Coles and R. Simon, (Ed. A. Blumstein), Polymeric Liquid Crystals, Plenum, New York 1983, p. 351.
35 T. Hatakeyama and Z. Liu, Handbook of Thermal Analysis, Wiley, Chichester 1998, p. 206.
36 H. Hatakeyama, T. Yoshida and T. Hatakeyama, J. Therm. Anal. Cal., 59 (2000) 157.
37 S. Nakamura, M. Todoki, K. Nakamura and H. Kanetsuna, Thermochim. Acta, 163 (1988) 136.
38 S. Hirose and H. Hatakeyama, Mokuzai Gakkaishi, 32 (1986) 621.
39 K. Nakamura, T. Hatakeyama and H. Hatakeyama, Polym. Adv. Technol., 3 (1992) 151.
40 J. H. Saunders and K. Fisch, in: Polyurethanes, Chemistry and Technology in High Polymers, Vol. XV, Interscience Publishers, New York 1962, p. 103.
41 K. V. Sarkanen and L. H. Ludwig Eds, Lignins, Wiley-Interscience, New York, 1971.
42 H. Hatakeyama, Y. Izuta, T. Yoshida, S. Hirose and T. Hatakeyama, Recent Advances in Environmentally Compatible Polymers (Eds J. F. Kennedy, G. O. Phillips, P. A. Williams and H. Hatakeyama), Woodhead Publishing, Cambridge 2001., p. 33.
43 M. L. Matsuzak and K. C. Frisch, J. Polym. Sci., Polym. Chem. Ed., 11 (1973) 637.
44 G. E. Domberg, G. A. Rossinskaya and A. I. Kalninsh, J. Thermal Anal., 2 (1972) 327.
45 G. E. Domberg, G. A. Rossinskaya and V. N. Sergreeva, J. Thermal Anal., 3 (1974) 211.